Flow Visualization of Natural Convection in a Tall, Air-Filled Vertical Cavity

J.L. Wright, H. Jin, K.G.T. Hollands, D. Naylor

Corresponding Author phone: (519) 888-4567 ext 6849
J.L. Wright, P.Eng. fax: (519) 888-5862
Professor jlwright@uwaterloo.ca
Department of Mechanical Engineering
University of Waterloo
200 University Avenue West, Waterloo, Ontario, Canada N2L 3G1

H. Jin, P.Eng.
Liburdi Engineering Ltd.
400 Highway 6 North
Dundas, Ontario, Canada, L9H 7K4

K.G.T. Hollands
Distinguished Professor Emeritus
Department of Mechanical Engineering
University of Waterloo
200 University Avenue West, Waterloo, Ontario, Canada N2L 3G1

D. Naylor, P.Eng.
Professor
Dept. of Mechanical & Industrial Engineering,
Ryerson University,
350 Victoria Street, Toronto, Ontario, Canada M5B 2K3

Abstract

Natural convection of air in a tall vertical cavity was studied using a smoke patterns and interferometry. Experiments covered Rayleigh numbers of $4{,}850 < Ra < 54{,}800$ and aspect ratio $A \approx 40$. Secondary cells were noted at Ra as low as 6,228. The flow was stable at $Ra < 10^4$. As Ra exceeded 10^4 the flow became irregular, the core flow became increasingly unsteady and 3-D motion became evident. Interferometry showed that most of the temperature drop exists in boundary layers near the walls. The core is well-mixed and of relatively uniform temperature with little or no vertical stratification.

Keywords

flow visualization, interferometry, natural convection, vertical cavity

Nomenclature

A	aspect ratio of cavity, dimensionless, H/L
C	a constant
C_p	specific heat at constant pressure of gas in cavity
g	gravitational acceleration
H	height of vertical cavity (x-direction), see Figure 1
H_c	vertical distance, centre-to-centre, between secondary cells
k	thermal conductivity of gas in cavity
L	cavity thickness (y-direction), see Figure 1
Nu	Nusselt number, dimensionless, see Equation 2
Pr	Prandtl number, dimensionless, $\mu C_p/k$
q''	average heat flux across cavity
Ra	Rayleigh number, dimensionless, $\rho^2 L^3 g C_p \Delta T \beta / \mu k$
Ra_c	critical Rayleigh number, dimensionless, see Equation 7
T_c	temperature of cold wall
T_h	temperature of hot wall

u, v horizontal and vertical components of velocity

v^* vertical component of velocity, dimensionless, $v/\sqrt{g\beta\Delta TL}$

v_{cell} velocity of secondary cell

v^*_{cell} velocity of secondary cell, dimensionless, $v_{cell}/\sqrt{g\beta\Delta TL}$

x,y,z Cartesian coordinates, see Figure 1

Greek symbols

α_c wave number of secondary cells, dimensionless, see Equation 8

β thermal expansion coefficient of gas in cavity

λ wavelength

μ dynamic viscosity of gas in cavity

ρ density of gas in cavity

ΔT temperature difference, T_h-T_c

1. INTRODUCTION

1.1 Background

Natural convection in a tall, air filled, vertical cavity has been studied with great interest because its relative simplicity and great practical importance. The literature includes evidence of research as long ago as 1909 [1] and a steadily increasing level of effort has since been devoted to experimental, analytical and computational study.

Figure 1 shows a cross-section of an air-filled vertical cavity, which is presumed to be long in the z-direction. The pertinent dimensions of the cavity are its height, H, and width, L. The temperatures of the hot and cold walls are T_h and T_c. The horizontal end walls are usually assumed to be either adiabatic (i.e., zero heat flux (ZHF)) or having a linear temperature profile (LTP). If the aspect ratio (A=H/L) of the cavity is large enough, the choice of ZHF or LTP boundary conditions has little influence on the total rate of heat transfer (e.g., [2, 3, 4]).

The scope of this study is restricted to rectangular cavities that are tall, vertical and air filled because specific information is sought regarding window glazing cavities. Various researchers (e.g., [5]) have shown that the solution, including velocity and temperature fields, can be stated in terms of the Rayleigh number, Ra, the Prandtl number of the fluid, Pr, and the aspect ratio of the cavity, A. In particular, the average rate of heat flux

across the cavity, q'', expressed in a dimensionless form as a Nusselt number, Nu, is given by the functional dependence:

$$Nu = Nu(Ra, Pr, A) \tag{1}$$

where $$Nu = q'' \frac{L}{k \cdot \Delta T} \qquad \Delta T = T_h - T_c \tag{2}$$

$$Ra = \frac{\rho^2 L^3 g C_p \Delta T \beta}{\mu k} \tag{3}$$

$$A = \frac{H}{L} \tag{4}$$

$$Pr = \frac{\mu C_p}{k} \tag{5}$$

Various fill gases are used in glazing cavities (e.g., air, Ar, Kr) but the Prandtl number does not differ appreciably from one gas to the next ($Pr \approx 0.71$). Measurements [6, 7] show that the influence of A on Nu is unimportant for A>25. Thus, Equation 1 can be simplified:

$$Nu = Nu(Ra) \tag{6}$$

In the context of glazing systems the upper limit on Ra, corresponding to a large indoor-outdoor temperature difference, is in the range of 6,000 to 10,000. It can be shown that an optimum pane spacing corresponds to Ra=8,104 [8,9].

1.2 Nature of the Flow at or Near $Ra=10^4$

Consider the measurements of ElSherbiny [6] and Shewen [10], shown in Figure 2 along with the correlation of Wright [8]. At very low Ra the flow is laminar, slowly ascending near the hot wall and slowly descending near the cold wall; viscous shear balances buoyancy forces and the heat transfer is dominated by conduction with $Nu \approx 1$. As Ra increases the flow moves more quickly and Nu departs from unity as the advection of energy across the ends of the cavity becomes more significant.

Two studies are regularly cited as pioneering work. Batchelor [5] provided significant insight into the phenomena associated with primary flow. Eckert and Carlson [11] used interferometry to quantify local heat transfer rates. These researchers discuss a variety of flow characteristics calling the situation characterized by Nu=1 the "conduction regime" and using the phrase "boundary layer regime" to describe the flow as Nu exceeds unity. In the conduction regime, with the exception of the regions near the ends of the cavity, a linear temperature profile exists. In the boundary layer regime the regions influenced by the flow reversals extend a greater distance from the ends of the cavity as Ra is increased and a vertical temperature gradient or thermal stratification extends into the core.

As Ra is increased further a multicellular flow arises. Korpela et al. [12] showed that the results of Bergholz [13] could be simplified to predict the

critical value of Grashof number at which the onset of secondary cells takes place from the conduction regime. This result, recast as a critical Rayleigh number is:

$$Ra_c = 8{,}000\left(1+\frac{5}{A}\right)\mathrm{Pr} \qquad (7)$$

Equation 7, using Pr=0.71, supplies a prediction of Ra_c=5,680 with A= ∞ and Ra_c=6,390 with A=40.

The presence of secondary cells within the core has been observed experimentally in several studies. A summary is presented in Table 1. Comments from two of these studies are of interest. Keizer-Boogh noted that cells were most easily seen at Ra≈8,700 because the smoke diffused quickly at higher values of Ra. Chikhaoui et al. mention that at higher values of Ra difficulties with "erratic fluctuations" were encountered.

Various researchers have undertaken stability analysis of secondary cells (e.g., [13, 14]) and it is regularly mentioned (e.g., [15]) that thermal stratification of the core suppresses the formation of secondary cells. Thermal stratification will be stronger in cavities of smaller aspect ratio and this influence can be seen in Equation 7. Lee and Korpela [4] indicate that secondary cells will not form in air-filled cavities of A<12. The increased strength of the primary flow at higher values of Ra will also increase the level of thermal stratification and accordingly the results of

stability analysis indicate that secondary cells will disappear as Ra becomes sufficiently large (e.g., [12, 14, 15, 16]). The vertical stratification is always strong, locally, at the ends of the cavity and this, in combination with the additional viscous damping adjacent the end-walls, ensures that secondary cells never form in these locations.

Table 1

Observation of Secondary Cells in the Tall, Vertical, Air-Filled Cavity

Researcher(s)	Ra	A	Method
Vest and Arpaci [17]	Gr=9,500 Ra ≈6,745	33	smoke streak patterns
Korpela [18]	Ra ≈6,390	33	smoke streak patterns
Keizer-Boogh [19]	8,700	14	cigar smoke
Chikhaoui et al. [20]	Ra≈7,100, Ra≈8,165	12	smoke
Lartigue et al. [21]	Ra=9,222	40	PIV, incense
Choi and Korpela [22]	Ra≈5,180, 6461, 8,946, 15,052	38.6	cigar smoke, annulus

1.3 Difficulties Encountered at $Ra>10^4$

Computational fluid dynamics (CFD) codes have been used to simulate natural convection in the tall vertical cavity by incorporating the assumption that the flow is two-dimensional (2-D), laminar and steady. Simulation results agree well with heat transfer measurements at low values of Ra but if the simulation is not able to resolve secondary cells (e.g., [3]) the predicted heat transfer rate falls low for values of Ra that

exceed Ra_c. If the simulation *is* able to resolve secondary cells (e.g., [4]) the predicted heat transfer rate agrees well with measured values for $Ra > Ra_c$ but only for a very small range of Ra and again falls low for $Ra > 10^4$ [4, 23, 24].

No clear explanation is offered for the discrepancy at $Ra > 10^4$ but clues appear in the literature. Keizer-Boogh [19], having found that visualization of secondary cells could most readily be accomplished at Ra=8,700 also mentioned that the flow was unsteady and the smoke used for visualization diffused quickly at higher values of Ra. Chikhaoui et al. [20] attempted flow visualization at Ra>8,165 but noted that the "flow structure appears to be unstable and becomes time dependent" and "... visualizations indicate rapid and erratic fluctuations suggesting a chaotic motion." CFD results generated by Lartigue et al. [21] show a very orderly distribution of local heat transfer and secondary cell distribution for Ra up to 10,102 but the corresponding distributions show noticeable disorder at Ra=14,200 and Ra=17,750. Eckert and Carlson [11] in their work using interferometry mention that "turbulent fluctuations could be observed in some of the test runs" at A=20 and $Gr > 10^4$ ($Ra > 7{,}100$). It was noted that these fluctuations had a comparatively low frequency and that the intensity of the fluctuations increased with Ra. Choi and Korpela [22] in their work with a tall vertical annulus observed that the flow was regular at Gr=12,600 ($Ra \approx 8{,}946$) but it was seen "to become irregular (and also

unsteady) as the Grashof number has been increased to 21,200" or Ra≈15,052. Lauriat and Desrayaud [14] completed numerical simulations using a 2-D formulation for A ranging from 10 to 40. They comment that, "Thousands of iterations were required sometimes (typically 2,000 at Gr=30,000 and A=20) because oscillations prevent the satisfaction of the convergence criterion. This behavior has been mentioned by Raithby and Wong". Wright [23] formulated a laminar, 2-D numerical simulation scheme. Comments regarding these simulations were offered by Wright and Sullivan [24]. It was noted that when simulations were performed at higher values of Ra (Ra=13,732 and Ra=16,479 at A=40) it was difficult to obtain convergence. In fact, the number of cells was changing, with cells appearing and disappearing and the flow adjusting as the numerical solver mimicked the progression through time. Stream function plots of the flow were irregular and this spatial disorder closely resembled the disorder shown in the images produced by Lartigue et al [21] for simulations in the same range of Ra. Wright and Sullivan [24] concluded that the simulation was not fully modeling all of the physical mechanisms of heat transfer for $Ra>10^4$.

1.4 Large Values of Ra

When Ra is sufficiently large the heat transfer is governed primarily by turbulent boundary layers, separated from each other by a core of uniform temperature, and the corresponding log-log plot of Nu versus Ra should

exhibit a slope of 1/3 (e.g., [25]). The experimental results shown in Figure 2 [6, 26] follow a 1/3 slope at Ra>50,000. The correlation shown in Figure 2 is of the form $Nu = C \cdot Ra^{1/3}$ at Ra>50,000 and closely follows the slope of the measured data.

Several numerical studies have explored the use of turbulence models. Almost all two-equation turbulence models over-predict the heat transfer [26, 27]. Ince and Launder [28] noted a "very satisfactory" agreement with experiment at $Ra>10^6$ but this high range of Ra is well beyond the values of Ra examined in this study.

1.5 Motivation and Objectives

The objective of this study was to investigate the flow patterns of air in a tall, vertical cavity with the specific goal of determining the capabilities that must be included in a numerical simulation if this problem is to be successfully modeled at $10^4<Ra<5x10^4$. Neither numerical simulation nor flow visualization has been accomplished in this range of Ra in which the transition from fully laminar to fully turbulent flow takes place.

2. APPARATUS AND METHODOLOGY

2.1 Apparatus

The test assembly consists of two aluminum plates, 1215 mm tall by 500 mm wide by approximately 17 mm thick. The cavity was constructed by

clamping one plate to the other with spacers at the perimeter. The spacers were made of transparent acrylic and were machined such that L = 28.90 mm. The aspect ratio of the cavity was A=40.8. The plate temperatures were maintained by two circulation loops connected to constant-temperature bathes. The temperature difference between the two plates was measured by a thermopile. The uncertainty in Ra for this experiment ranged from about 5% at Ra=4,850 to less than 2% at Ra=54,800 [29]. Ra was varied by adjusting the temperature difference between ΔT=1.82 K and ΔT=24.86 K.

2.2 Smoke Flow Visualization

The apparatus is shown in Figure 3. Smoke was generated using a smoke tube. (actually a sulphuric acid aerosol generated by a Dräger smoke tube, model: Air Current CH25301, AFC International Inc.) The smoke was introduced through the bottom spacer.

A 10 mW helium-neon laser (Uniphase 1125P) was positioned above the cavity. Lenses were used to obtain a vertical sheet of laser light perpendicular to the bounding plates.

Smoke streaks in the laser sheet illustrated the flow pattern in two dimensions. These patterns were then captured by a video camcorder which was, in most cases, aimed at the middle section of the cavity.

2.3 Visualization Using Interferometry

A 20 cm diameter beam Mach-Zehnder interferometer, fitted with a 10 mW He-Ne laser, was used to visualize the temperature field in the cavity. In all cases, the interferometer was operated in the infinite fringe mode. In this mode, the lines of constructive and destructive interference in the output (called fringes) can be interpreted as isotherms, when measurements are made in a 2-D temperature field. General information on the operational principles and setup of laser interferometers is given by Hauf and Grigull [30] and Naylor [31]. A more detailed description of the interferometer used in the present experiment is offered by Machin et al. [32].

Experiments were undertaken to record interference patterns at two locations: the middle section and the top end of the cavity. For these tests, a section of the acrylic spacer was replaced with a high precision optical window on each side of the cavity. The transient fringe patterns were recorded using a digital video camcorder.

3. VISUAL OBSERVATIONS

3.1 Smoke Flow Visualization

Streak flow patterns were observed at the center of the cavity and the corresponding photographs are shown in Figures 4 through 10. All photographs have been cropped such that their edges correspond to the

vertical cavity walls. The length scale in each picture can be estimated by the reference dimension, L=28.9 mm. The left edge of each picture corresponds to the hot wall, and the right edge corresponds to the cold wall.

3.1.1 Ra = 4,850 to 6,220 (Conduction Regime)

The unicellular flow was captured by the smoke visualization, and found to be slow and stable. The flow at values of Ra up to and including Ra=6,220 was observed to be steady. The speed of the flow increased as Ra was increased. No secondary cells were seen.

3.1.2 Ra≈6,800 (Transition to Secondary Flow)

The critical Ra predicted, for this experiment, by Equation 7 is Ra_c=6,376. Secondary flow was observed at Ra=6,819 but not at Ra=6,220. The secondary cells co-rotate with the primary flow. See Figure 4. The primary flow was stable along the walls, and at Ra=6,819 was closer to the walls relative to its position at Ra≈6,220.

Both primary flow and secondary flow were time-steady with the exception that the secondary cells moved slowly downward at a rate of $v_{cell} \approx 3.4 \frac{mm}{\sec}$.

The secondary cells are long in the vertical and narrow in the horizontal direction, and are similar to, but not as regular as, the cat's eye pattern predicted numerically.

3.1.3 Ra≈7,300 to 8,600 (Stable Secondary Flow)

The flow pattern in this Ra range is similar to the flow pattern at Ra≈6,800. With the increase of Ra from 7,300 to 8,600, the following observations were made: (1) The primary flow moved closer to the walls and the velocity of the primary flow increased. (2) All cells continued to co-rotate with the primary flow. The secondary flow became stronger. The rotational velocity of secondary cells and the velocity at which secondary cells move downward increased with the increase of Ra. At Ra≈8,600, the cells moved downward at a rate of about $v_{cell} \approx 9.8 \frac{mm}{\sec}$, which is approximately three times faster than the corresponding motion at Ra≈6,800. (3) Very small fluctuations with time were observed. They took the form of a slight waviness in the primary flow streak lines. (4) The dimension of the secondary cells shortened in the vertical and widened in the horizontal; that is, the shape of secondary cells became more rounded.

3.1.4 Ra≈9,600 to 10,500 (Secondary Flow Unstable)

With Ra increased to approximately 10^4, the flow in the core started to become unstable; that is, the flow pattern was frequently disrupted by

secondary cell movements. The secondary cells were moving and rotating faster and their influence on the adjacent fluid was more pronounced. The direction of cell motion was no longer always downward; rather it was subject to a tendency for the cells to make irregular excursions from-side-to-side, and with respect to a frame of reference attached to the general downward movement, up and down. On some occasions the disturbance involved the interaction of two cells, these two cells generally moving in opposite directions, toward opposite walls. A limited amount of three-dimensional (3-D) variation in the flow was first observed in this range of Ra as cells would suddenly disappear from the plane of the laser light.

3.1.5 Ra≈11,600 to 12,600 (3-D Flow Exhibited)

In this range of Ra, the cell movements were more frequently found to be 3-D, indicated by the frequent appearance or disappearance of flow features from the laser sheet. The magnitude of flow disruption in these disturbances increased with the increase of Ra. Cells were found to have a variety of sizes and shapes. The velocities increased with Ra. The layer of primary flow next to the walls became thinner. Strongly rotating cells were present and their movement often disrupted the primary flow. The direction of cell movement was generally random, although there was a weak downward trend. It was readily apparent that flow in this range of Ra is 3-D, even though it is difficult to discern 3-D flow using 2-D imagery. Although the flow had become 3-D, the magnitude of flow in the third

dimension, in such a narrow cavity, appeared small compared to the movement in the vertical direction.

3.1.6 Ra≈13,600 to 54,800 (Transition to Fully Turbulent Flow)

In the Ra range from 13,600 to 25,100, the magnitude of 3-D fluctuations was found to increase further with the continued increase of Ra. The flow became more and more chaotic and turbulent - moving faster and more vigorously. The flow was dominated by the random movements of cells. All cells observed were co-rotating with different length scales. See Figure 5. As Ra was increased to 54,800, the flow was observed to be fully turbulent with strong turbulent eddy movements. See Figure 6. The average size of the turbulent eddies has a tendency to decrease with the increase of Ra. The turbulent eddies were generated everywhere in the cavity. The strain rate was observed to be very high. The following are several observations regarding features of the turbulent cells:

- Co-rotating and Counter Rotating Cells: In the transition to turbulence, most cells or turbulent eddies are co-rotating with the primary flow. See Figure 7. With Ra increased beyond 30,000, counter co-rotating eddies were also found. See Figure 8.

- Compound Cells: Some pairs of small cells were observed to merge, forming one larger cell in a compound structure with small cells wrapped inside. See Figure 9.

- Length Scales: Cells (eddies) with significant momentum were found to form at smaller sizes, compared to the secondary cells that exist at lower values of Ra. In general, the size at which eddies were formed decreased with Ra. Cells generally dissipated at smaller length scales. See Figure 10. However, some cells appeared to grow larger before dissipating. See Figure 11.

4. DISCUSSION OF SMOKE/LASER FLOW VISUALIZATION

4.1 Motion of Secondary Cells

The presence of secondary cells at $Ra_c < Ra < 10^4$ was expected but the downward motion of these cells was unexpected. Stability theory predicts a "stationary" disturbance at Ra_c. Numerical simulations show an array of cells – each remaining in a single location. This characteristic of the converged solution results not so much from the fact that a numerical scheme may have been formulated to arrive at a steady-state solution but because the centro-symmetry of the problem precludes the possibility of observing an asymmetry such as the migration of secondary cells from one end of the cavity to the other. The same point can be made in a different way. It is common for "steady-state" simulations to march through time, although this progression might entail a distorted transient, as an iterative solver progresses toward a converged solution. Thus, one might expect to find evidence of cell motion if successive samples of the unconverged

velocity field were examined. However, this effort is almost certain to be unsuccessful if evidence of an asymmetric motion is sought. A numerical simulation scheme can be expected to retain the symmetry of the problem. Each numerical manipulation executed with respect to any given location in the flow will be repeated for the corresponding location of symmetry. A very good example can be found in the work of Wright and Sullivan [24] who devised a numerical scheme whereby secondary cells were triggered by perturbing the primary flow. As the solver worked toward a steady-state solution cells were sometimes created or sometimes lost – but always in pairs. If a cell disappeared at one end of the cavity the corresponding cell would simultaneously disappear at the other end of the cavity. This led to the peculiarity that if an odd or even number of cells were created by the perturbation, the final solution would include an odd or even number of cells, respectively – and never vice-versa.

However, it is not unreasonable to expect movement of cells if for some reason the centro-symmetry is lost. Three possibilities come to mind, all of which present themselves in experimental work although the resulting departure(s) from symmetry may be immeasurably small. First, initial conditions may differ. Small perturbations, such as vibration, may alter the flow. This situation is unlikely and no evidence of this effect is apparent in the literature. Second, an asymmetry in the geometry might result in cell motion. A good example is a cavity that is not perfectly

vertical. Another example can be seen in the work of Choi and Korpela [22] who observed secondary cells in a tall vertical cavity, but their cavity did not have centro-symmetry because it was annular, and upward cell motion was observed. Third, the fact that fluid properties are temperature-dependent may create a sufficient departure from centro-symmetry for cell motion to be initiated.

Motion of secondary cells was observed independently by Lartigue-Dasquet [33]. Cells were found to move downward at a speed of $v_{cell} = 1.30 \frac{mm}{sec}$ during experiments conducted with air in a cavity of aspect ratio A=40 (L=15 mm) at Ra=9,222. A matching numerical simulation was completed, using a formulation that included temperature-dependent fluid properties, while retaining the Boussinesq approximation, and secondary cells were found to drift downward at a speed of $v_{cell} = 1.34 \frac{mm}{sec}$. These two results are in very good agreement with each other. The reference velocity, $\sqrt{g\beta\Delta TL}$, was used to scale these cell speeds and they were presented in dimensionless form by Lartigue et al. [21]: $v^*_{cell} = 0.0107$ and $v^*_{cell} = 0.0110$. Converting the cell speeds observed in the current study to the same dimensionless form, $v_{cell} = 3.4 \frac{mm}{sec}$ at Ra=6,800 and $v_{cell} = 9.8 \frac{mm}{sec}$ at Ra=8,600 become $v^*_{cell} \approx 0.07$ and $v^*_{cell} \approx 0.17$. These results show the trend of increasing cell speed that might be expected at larger values of Ra but

they differ from the values found by Lartigue. It is tempting to speculate about the reason for this difference but it should be pointed out that the overriding impression, in viewing the flow, is that not only is the secondary flow weak but the motion of the cells is slow. Lartigue et al. [21] mention that the speed of the cell motion observed in their study was about 1% of the maximum velocity of the primary flow. Clearly, the flow in the core is governed by a delicate balance of forces. In fact, a small increase in Ra beyond $Ra=10^4$ produced evidence of more irregular cell motion that was not uniformly downward. In subsequent experiments using incense, that have not yet been reported, secondary cells were seen to move upward.

4.2 Size of Secondary Cells

The size of the secondary cells can best be measured as the vertical centre-distance between adjacent cells, H_c, and expressed in a dimensionless form as, H_c/L. This information can also be expressed as a dimensionless wave-number, α_c.

$$\alpha_c = 2\pi \frac{L}{H_c} \tag{8}$$

The theoretical wave-number for cells at $Ra=Ra_c$ and $A\rightarrow\infty$ is $\alpha_c=2.8$ [13]. Lee and Korpela [4] completed simulations with A=20 giving $\alpha_c=2.82$ at Gr=11,000 ($Ra\approx7,800$) and their numerical results show that the cells

lengthen (i.e., α_c will diminish) as Ra is increased. Lartigue et al. [21] measured $\frac{H_c}{L} = \frac{3.95\,cm}{1.5\,cm} = 2.6$ giving α_c=2.39 at Ra=9,222.

Estimates of H_c are difficult to make on the basis of the current smoke streak observations – to some extent because of the irregular nature of the flow at values of Ra as low as Ra=9,600. Nonetheless, Jin [29] gave crude estimates of $\frac{H_c}{L} \approx 1.5$ ($\alpha_c \approx 4.2$) at Ra=9,600 and $\frac{H_c}{L} \approx 2$ ($\alpha_c \approx 3.14$) at Ra=8,600. Jin did not offer an estimate of cell spacing at Ra=6,800 but re-examination of the photographs made by Jin [29] reveals that $\frac{H_c}{L} \approx 2$ at Ra=6,800. The more compact spacing of secondary cells, as Ra is increased from 6,800 to 9,600 can be seen in Figure 4.

Observations made by Lartigue et al. [21] agree reasonably well with cell spacings predicted by the stability theory of Bergholz [13] and the simulation results of Lee and Korpela [4], although this comparison is not ideal because of mismatches in Ra and A. The current observations, ranging from $\alpha_c \approx 3.14$ to $\alpha_c \approx 4.2$, show a tighter spacing of cells than observed by the other researchers. This can be taken as a reminder that the nature of the flow in the core is governed by a very delicate balance of forces. Recall that Wright [23, 24] could produce several different solutions numerically, including different numbers of cells, for identical

values of Ra and A. The more important observation is that the streak flow patterns show shorter and rounder cells, in a more tightly spaced sequence as Ra is increased whereas Lee and Korpela [4] predicted the opposite behaviour on the basis of numerical simulation. Numerical simulation may not be fully characterizing the true nature of the flow at $Ra_c < Ra < 10^4$ even though the predicted values of Nu are accurate.

4.3 Simulation Requirements

The flow of gas in the tall, vertical slot can be treated as 2-D, laminar and steady at $Ra < 10^4$ and CFD codes formulated to characterize this type of flow are common. A unicellular primary flow exists until Ra exceeds Ra_c ($Ra_c \approx 6{,}000$). In the range of $Ra_c < Ra < 10^4$ the numerical model must be able to resolve secondary cells and various techniques to satisfy this requirement have been demonstrated (e.g., [4, 23, 24, 33]). A CFD model that provides a steady-state solution will not account for the possibility of cell motion and the number/size of secondary cells in the solution may not correspond perfectly to reality but the secondary flow is generally weak to the extent that fine details concerning the nature of the cells do not strongly influence the average or local heat transfer. In their 3-D numerical simulation Chikhaoui et al. [20] resolved secondary cells (A=12) but also predicted the flow field to be 3-D at $Ra \approx 8{,}165$. Visualization did not offer evidence of the strong transverse motion predicted by Chikhaoui

et al. Indeed, it has been well demonstrated that a 2-D, laminar, steady model is satisfactory for predicting heat transfer rates for $Ra_c < Ra < 10^4$.

Once Ra exceeds 10^4 the requirements of a numerical simulation are significantly different. Flow visualization has shown that the core becomes increasingly chaotic as the transition to turbulence takes place; $10^4 < Ra < 5x10^4$. The numerical model will need to account for a 3-D unsteady flow. The inability to predict heat transfer rates using a 2-D, laminar, steady simulation in this range of Ra is evidence that the disruption in the core cannot be ignored. However, it is expected that a traditional two-equation, time-averaged, turbulence model is not well suited to this problem. It is unlikely that turbulence exists in the boundary layers until Ra exceeds $5x10^4$ and attempts to apply a two-equation model have been unsuccessful even at higher values of Ra. Instead, it appears that the transition can best be modeled using Direct Numerical Simulation (DNS) to reproduce the unique characteristics of the flow in the core.

Phillips [34] used DNS to a simulate a vertical slot (i.e., unstratified) at two values of Ra – one of which falls just outside the range of interest here. Predicted values of Nu (2.22 and 3.36) were lower than measurement by approximately by 22% and 14% at Ra=64,800 and Ra=180,000, respectively[+]. Nonetheless, Phillips offers some key information. One of

[+] There is some confusion on this point. Phillips [32] states that "The computed Nusselt numbers are about 25% higher than the commonly available correlations ..."

the most interesting aspects of Phillips' work is that a visual representation of an isothermal surface was produced (Ra≈64,800) and this figure has a striking similarity to the chaotic flow field observed in the current visualization work. In addition, Phillips [34] used DNS results to examine turbulence statistics and two important points can be made on the basis of these results. First, his data support to the idea that the boundary layer does not become turbulent until Ra exceeds $5x10^4$. While discussing the dimensionless Reynolds normal stresses Phillips stated, "The v^2 component has a peak near the slot center and is weak near the slot walls. This indicates that the turbulence is primarily originating from the shear layer at the slot center as opposed to the boundary layers near the slot walls which are more stable." Second, Phillips shows that the wavenumbers of eddies in the turbulent core span a very narrow range – less than two orders of magnitude. This coincides with the general impression that eddies seen during visualization were predominantly large (i.e., length scale of the same order as the width of the core) and this characteristic of the flow supports the idea that DNS will be well suited to the simulation of this problem at $Ra>10^4$.

5. OBSERVATIONS BASED ON INTERFEROMETRY

Interferometry was undertaken over the range of Ra for which cells were observed in the smoke flow visualization. This was done in order to compare the two sets of information and learn about the interferometry patterns that result from some of the more complex flow fields. Specifically, interferometry was carried out at values of Ra ranging from 7,800 to 54,200.

Fringe patterns in two sections of the cavity were recorded by a digital video camcorder, with the interferometer optics set in the infinite fringe mode. Interferograms taken in the middle section of the cavity (the same position as smoke flow visualization experiment) are shown in Figures 12 and 13. The high temperature wall is on the left. Figure 14 includes photographs of flow at the top end of the cavity. Unlike the photographs of smoke visualization, the cavity walls were not cropped from the interferometry images but the vertical walls are readily apparent.

It is known that fringes (i.e., isotherms) will appear through the centre section of the cavity as a set of vertical lines for values of Ra that fall within the conduction regime. In this situation the temperature profile across the cavity is linear and the fringes will be equally spaced. The presence of secondary cells can be expected for the lowest value of Ra for which interferometry was completed; Ra=7,800. The interferogram for

Ra=7,800 shows a set of vertical fringes. See Figure 12. These fringes are very nearly equally spaced and this is in keeping with the fact that Nu is only marginally greater than unity (Nu≈1.16 at Ra=7,800). In addition, the fringes were not steady but moved with a wavelike character.

In a general sense, the fringe patterns were observed to be similar for all values of Ra ranging from 7,800 (secondary cells) to 54,200 (highly chaotic). The fringe lines became more concentrated near the vertical walls at higher values of Ra, indicating high temperature gradients near the walls and a more uniform temperature field in the core of the cavity. The tightly spaced fringes near the walls were observed to be steady but the fringes in the core were unsteady - the magnitude and frequency of the fluctuations increasing with increases in Ra.

The fringe patterns are highly skewed and quite stable in the end regions of the cavity. See Figure 14. No qualitative difference was seen in these locations with changes in Ra. The highest temperature gradients, at any given value of Ra, were observed at the bottom of the hot wall and at the top of the cold wall.

6. DISCUSSION OF INTERFEROMETRY

It is clear, particularly from the interferograms for $Ra>2x10^4$, that two boundary layers exist at the vertical walls of the cavity. As Ra is increased the boundary layers pull closer to the walls, the temperature gradient at

the walls increases and Nu increases accordingly. The highest temperature gradients, and the highest local values of Nu, are found near the "leading" corners where each boundary layer begins to develop. These phenomena coincide with a significant amount of established information based on theory, experimentation and numerical analysis.

It is striking that interferometry gives so little information regarding the nature of the velocity field. For instance, at Ra=7,800 the fringe patterns display a wavelike character but these waves give little information about the underlying pattern of secondary cells. Of course, the fact that the secondary cells may be moving and causing the fringes to appear with moving waves instead of stationary waves, only confuses the issue. Similar isotherm patterns, waves included, have been produced by numerical simulation but in each instance charts of the flow field are available (e.g., streamline plots) and the temperature field viewed in this context is more easily understood. The simplicity of the fringe pattern produced by interferometry is deceiving.

More vivid examples of how the interferometry can mislead are seen in fringe patterns produced at $Ra>10^4$. Smoke/laser visualization showed that these flows include a significant amount of chaotic motion. The flow is increasingly unsteady and three dimensional as Ra is increased from 10^4 to $5x10^4$. Cells appear, move and dissipate. Some evidence of this highly pronounced chaotic disorder was expected in the interferometric

images but little was found. Instead, clear evidence of stable boundary layers was found and the only hint of disorder was presented by the wavelike motion of the fringes through the core. One could easily conclude that the flow is two-dimensional, albeit unsteady, on the basis of inteferometry, but the flow is not 2-D. Interferometry was unable to resolve the detail associated with cells and chaotic motion. The reason for this can be understood by recognizing that the density measured by a given parcel of light is influenced by all of the fluid encountered over the length of its path within the test section. Therefore, the resulting fringe plot represents a temperature map based on an integrated measurement through the depth of the test section and local variation of temperature is masked by this spatial averaging. A more detailed discussion of this effect is given by Naylor and Machin [35].

The flow in the end regions of the cavity was found to be steady and well behaved. This observation was clear from the smoke/laser visualization and the interferometry gives no evidence to the contrary. As expected, the temperature field is heavily skewed to one side of the cavity in the end regions because of the relatively strong advection across the cavity as the flow crosses over and a new boundary layer develops. A high temperature gradient exists in the "starting corner" of the boundary layer. This contributes to the formation of condensation on the bottom, indoor surfaces of windows a cold climate.

Thermal stratification of the core was not expected because of the large aspect ratio of the cavity. No evidence of stratification can be seen in the interferometric images - although it should be noted that stratification would need to be reasonably strong if it were to be detected over the short section of the cavity that can be seen in each image.

7. CONCLUSIONS

The secondary flow pattern was observed clearly at Ra=6,819 while no cells were found at Ra=6,228. This finding agrees with the stability analysis of Bergholz [13] that predicts Ra_c=6,376 for a cavity with aspect ratio A=40.8. In contrast with the results of numerical simulation, the secondary cells were observed to become more closely spaced as Ra was increased beyond Ra_c. Secondary cells are not perfectly steady (i.e., stationary) at any value of Ra and relative order is replaced by increasing levels of disorder as Ra exceeds 10^4. Interferometry detected secondary cells only to the extent that a wavelike disturbance was seen in the core. Although the presence of secondary cells will augment the heat transfer across the cavity (by 10% at most) there is evidence that the shape, spacing and bulk motion of secondary cells have little influence in this regard.

Flow in the core is chaotic and includes 3-D characteristics in the range of $10^4<Ra<5x10^4$. The flow moves more quickly and disturbances are more random and more pronounced as Ra is increased. The length scales of the

cells decreases at higher values of Ra. Most cells were found co-rotating while counter-rotating cells were observed at $Ra>3x10^4$. Interferometry shows stable boundary layers that pull more closely to the vertical walls as Ra is increased. Most of the temperature drop exists in the boundary layers while the core is well mixed and retains a relatively uniform temperature. Again, wavelike disturbances were seen in the interferometric fringe plots but detail regarding the chaotic nature of the velocity field was not evident. The flow in the core could readily be described as turbulent as Ra approaches $5x10^4$ but no indication of turbulence in the boundary layers was seen. Little or no stratification of the core was observed.

Numerical simulation based on a steady, laminar flow model is able to predict Nu for $Ra<10^4$ providing secondary cells can be resolved. In the transition from $Ra=10^4$ to $Ra=5x10^4$ disturbances in the core cannot be reproduced by this type of model and predictions of Nu fall below measured heat transfer rates. It is proposed that a DNS formulation is needed to account for the chaotic and 3-D nature of the flow and in turn predict more accurate values of Nu.

ACKNOWLEDGEMENTS

This research was supported by the Natural Sciences and Engineering Research Council of Canada.

REFERENCES

1. W. Nusselt, *V.D.I. ForschArb*. Nos 63 and 64, 78. (1909)

2. P. LeQuéré, T.A. de Roquefort, Transition to unsteady natural convection of air in differentially heat vertical cavities, HTD-Vol. 60, ASME. (1986)

3. G.D. Raithby, H.H. Wong, Heat transfer by natural convection across vertical air layers", Numerical Heat Transfer 4, (1981) 447-457

4. Y. Lee, S.A. Korpela, Multicellular natural convection in a vertical slot, *Journal of Fluid Mechanics* 126 (1983) 91-212

5. G.K. Batchelor, Heat transfer by free convection across a closed cavity between vertical boundaries at different temperatures, *Quarterly of Applied Mathematics*, Vol. XII (1954) 209-233

6. S.M. ElSherbiny, Heat transfer by natural convection across vertical and inclined air layers, Ph.D. thesis, University of Waterloo, Canada, 1980.

7. S.M. ElSherbiny, G.D. Raithby, K.G.T. Hollands, Heat transfer by natural convection across vertical and inclined air layers, *Journal of Heat Transfer* 104 (1982) 96-102

8. J.L. Wright, A correlation to quantify convective heat transfer between between vertical window glazings, *ASHRAE Transactions* 102 (1) (1996) 940-946

9. K.G.T. Hollands, J.L. Wright, C. Granqvist, Glazings and Coatings, In *Solar Energy: The State of the Art* (Edited by J.M. Gordon), Chap 2. James and James, London (2001)

10. E.C. Shewen, A peltier effect technique for natural convection heat flux measurement applied to the rectangular open cavity, Ph.D. thesis, University of Waterloo, Waterloo, Canada, 1986.

11. E.R.G. Eckert, W.O. Carlson, Natural convection in an air layer enclosed between two vertical plates with different temperatures, *International Journal of Heat and Mass Transfer* 2 (1961) 106-120

12. S.A. Korpela, Y. Lee, J.E. Drummond, Heat transfer through a double pane window, *Journal of Heat Transfer*, Trans. ASME 104, (1982) 539-544

13. R.F. Bergholz, Instability of steady natural convection in a vertical fluid layer, *Journal of Fluid Mechanics* 84 (4) (1978) 743-768

14. G. Lauriat, G. Desrayaud, Natural convection in air-filled cavities of high aspect ratio: discrepancies between experimental and theoretical results, 85-HT-37, Proceedings of the National Heat Transfer Conference, ASME, 1985.

15. G. de Vahl Davis, I.P. Jones, The effect of vertical temperature gradients on multi-cellular flows in high aspect ratio cavities, Conference on Liquid Metal Technology in Energy Production, Oxford, April 9-13., 1984.

16. R. Roux, J.C. Grondin, P. Bontoux, G. de Vahl Davis, Reverse transition from multicellular to moncellular motion in vertical fluid layer, Physics Chemical Hydrodynamics, European Physical Society, Madrid, March 30 – April 2, 1980.

17. C.M. Vest, V.S. Arpaci, Stability of natural convection in a vertical slot, *Journal of Fluid Mechanics* 36 (1) (1969) 1-15

18. S.A. Korpela, A study of the effect of Prandtl number on the stability of the conduction regime of natural convection in an inclined slot, *International Journal of Heat and Mass Transfer* 17 (1974) 215-222

19. E.M. Keizer-Boogh, Numerieke berekening van de k-waarde van dubbel glas, Faculteit der Technische natuurkunde, Technische Universiteit Delft, 1984.

20. A. Chikhaoui, J.F. Marcillat, R.L. Sani, Successive transition in thermal convection within a vertical enclosure, Natural Convection in Enclosures, HTD-Vol. 99, ASME, (1988)

21. B. Lartigue, S. Lorente, B. Bourret, Multicellular natural convection in a high aspect ratio cavity: experimental and numerical results, *International Journal of Heat and Mass Transfer* 43 (2000) 3157-3170

22. I.G. Choi, S.A. Korpela, Stability of the conduction regime of natural convection in a tall vertical annulus, *Journal of Fluid Mechanics* 99 (1980) 725-738

23. J.L. Wright, The measurement and computer simulation of heat transfer in glazing systems, Ph.D. thesis, University of Waterloo, Waterloo, Canada, 1990.

24. J.L. Wright, H.F. Sullivan, A two-dimensional numerical model for natural convection in a vertical, rectangular window cavity, *ASHRAE Transactions* 100 (2) (1994) 1193-1206

25. G.D. Raithby, K.G.T. Hollands, T.E. Unny, T.E., Analysis of heat transfer by natural convection across vertical fluid layers, *Journal of Heat Transfer* 99 (1977) 287-293

26. P.L. Betts, A.A. Dafa'Alla, Turbulent buoyant air flow in a tall rectangular cavity, Significant Questions in Buoyancy Affected Enclosure or Cavity Flows, HTD-Vol. 60, ASME (1986) 83-91

27. R.A.W.M. Henkes, Natural-convection boundary layers, Ph.D. thesis, Delft University of Technology, Delft, The Netherlands, 1990.

28. N.Z. Ince, B.E. Launder, B.E., On the computation of buoyancy-driven turbulent flows in rectangular enclosures, *International Journal of Heat and Fluid Flow* 10 (2) (1989) 110-117

29. H. Jin, Flow visualization of natural convection in a vertical cavity, M.A.Sc. thesis, University of Waterloo, Waterloo, Canada, 2000.

30. W. Hauf, U. Grigull, Optical methods in heat transfer, In *Advances in Heat Transfer*, (Edited by J.P. Harnett, T.F. Irvine Jr.), pages 133-366, Academic Press Inc., New York, 6, (1970)

31. D. Naylor, Recent developments in the measurement of convective heat transfer rates by laser interferometry, *International Journal of Heat and Fluid Flow*, 24, (2003) 345-355.

32. A.D. Machin, D.S. Naylor, J. Harrison, P.H. Oosthuizen, Experimental study of free convection at an indoor glazing surface with a venetian blind, *International Journal of HVAC&R Research* 4 (2) (1998)153-166

33. B. Lartigue-Dasquet, Contribution a l'etude thermique et dynamique de doubles vitrages courbes. approche numerique et experimentale", Ph.D. thesis, L'Institut National des Sciences Appliquees de Toulouse, France, 1999.

34. J.R. Phillips, Direct simulations of turbulent unstratified natural convection in a vertical slot for Pr=0.71, *International Journal of Heat and Mass Transfer* 39 (12) (1996) 2485-2494

35. D. Naylor, A.D. Machin, The accuracy of beam-averaged interferometric temperature measurements in a three-dimensional field, *Experimental Heat Transfer* 14, (3) (2001) 217-228

List of Figures

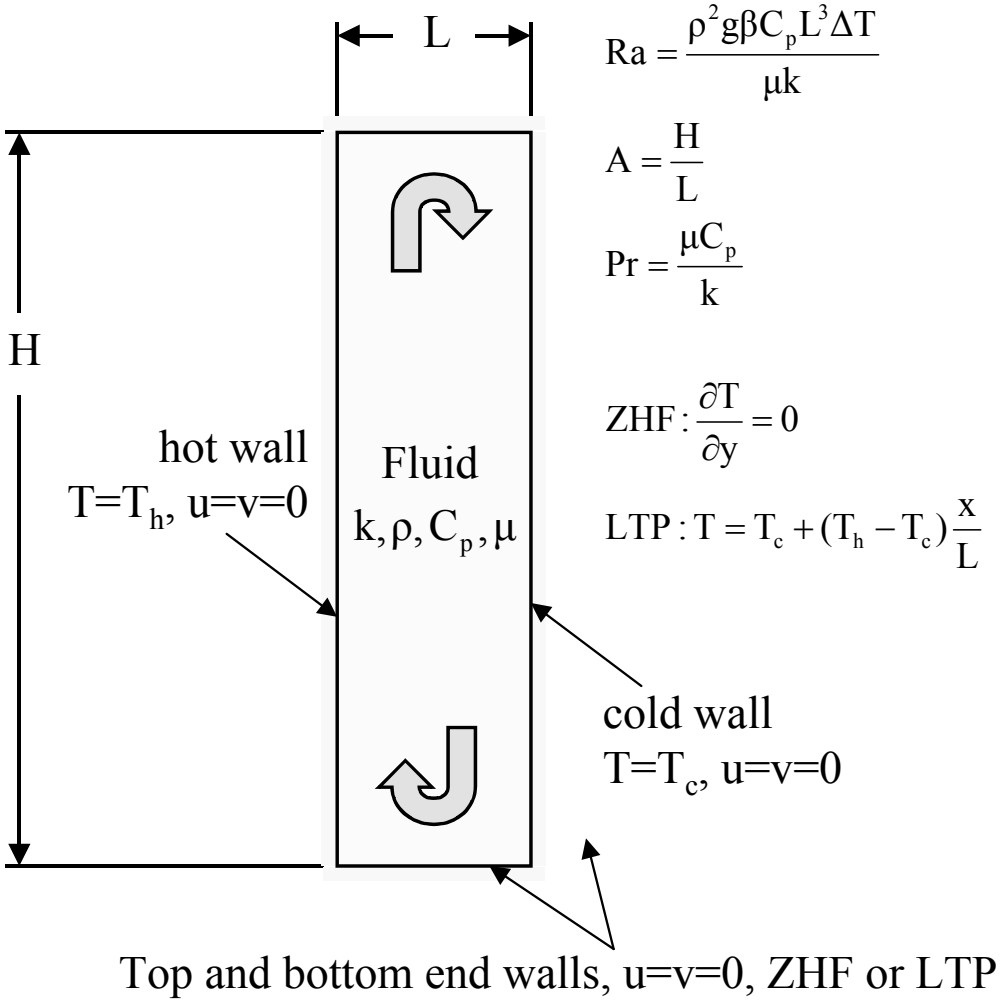

Figure 1: Schematic of the Vertical Cavity

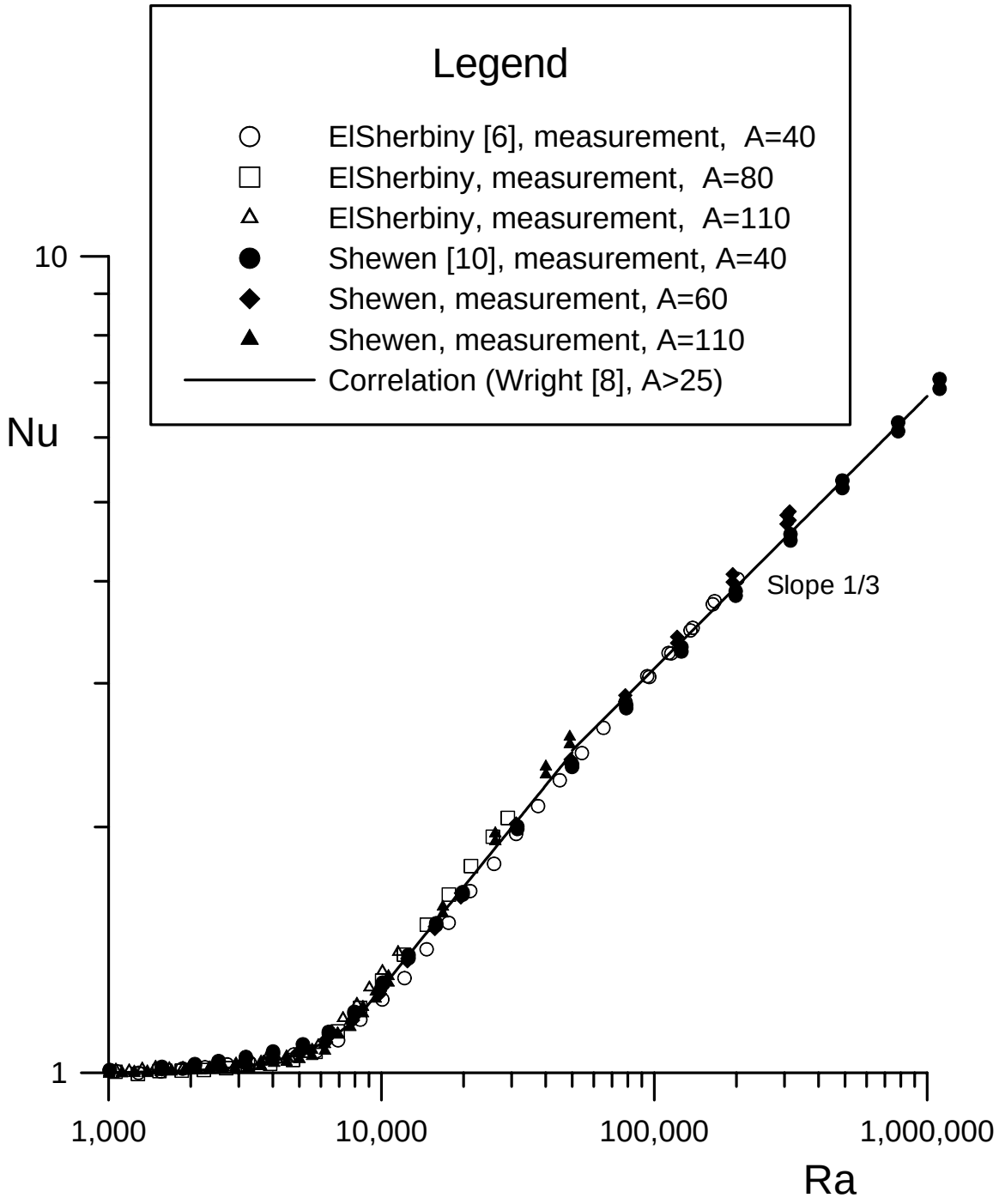

Figure 2: Nu versus Ra: Measurements of ElSherbiny [6] and Shewen [10] and Correlation of Wright [8]

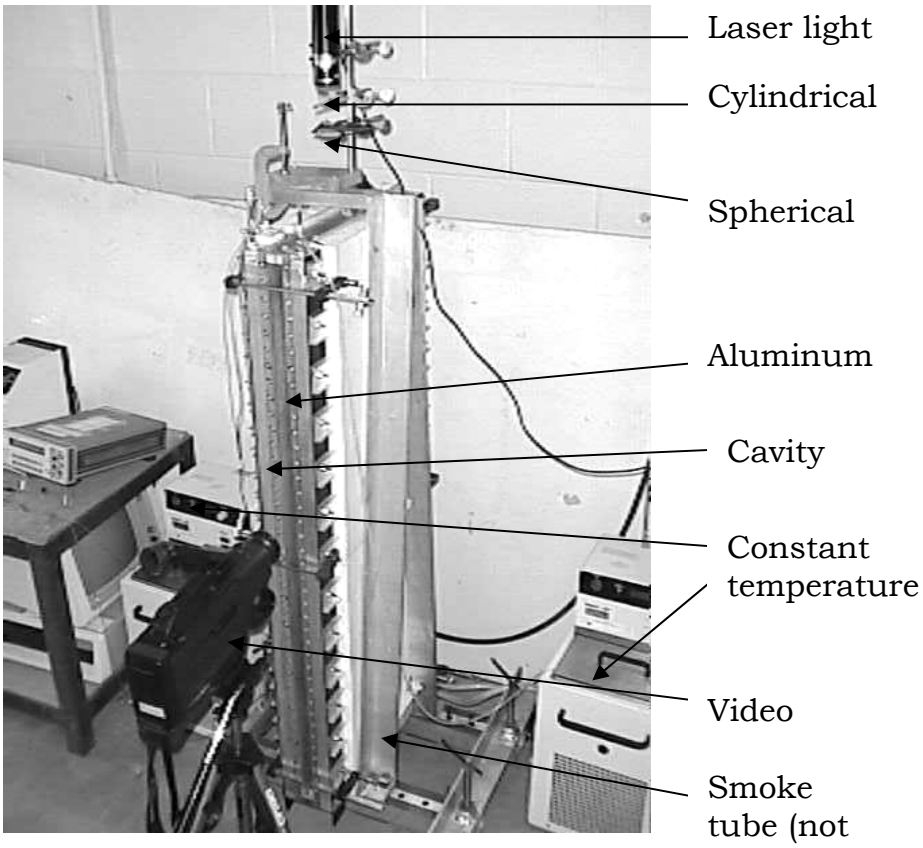

Figure 3: The Flow Visualization Apparatus

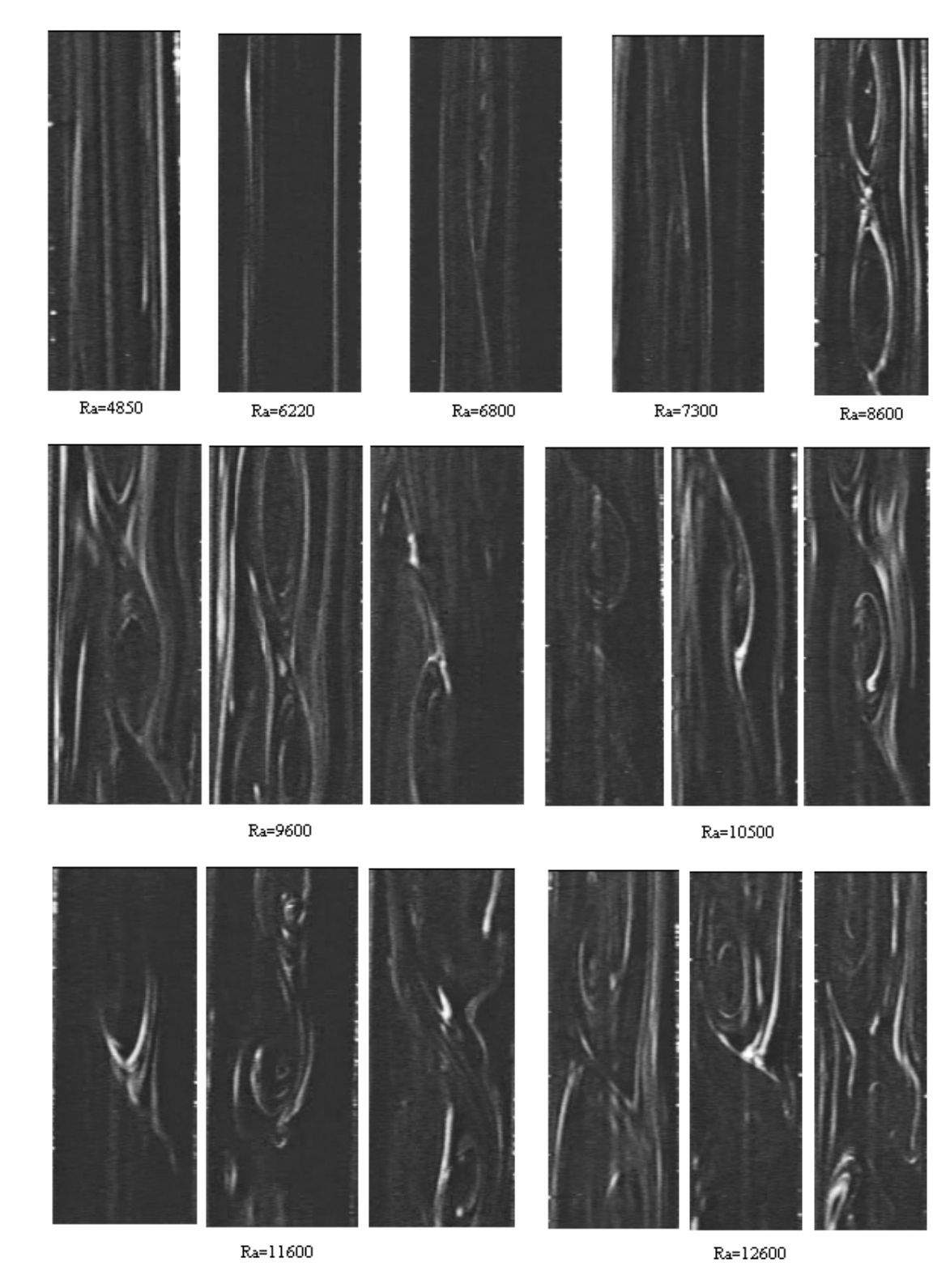

Figure 4: Streak Flow Pattern at Ra from 4,850 to 12,600

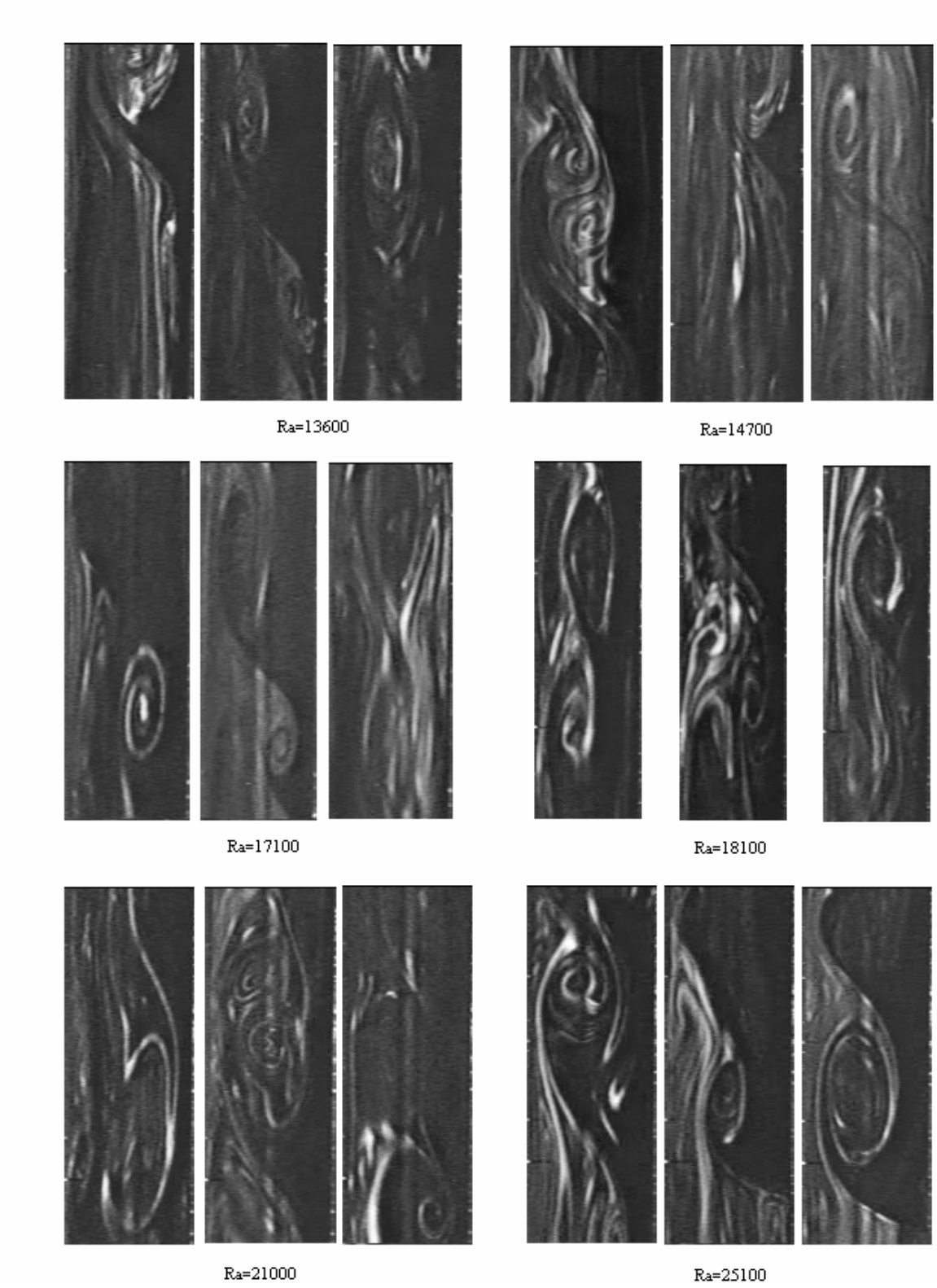

Figure 5: Streak Flow Pattern at Ra from 13,600 to 25,100

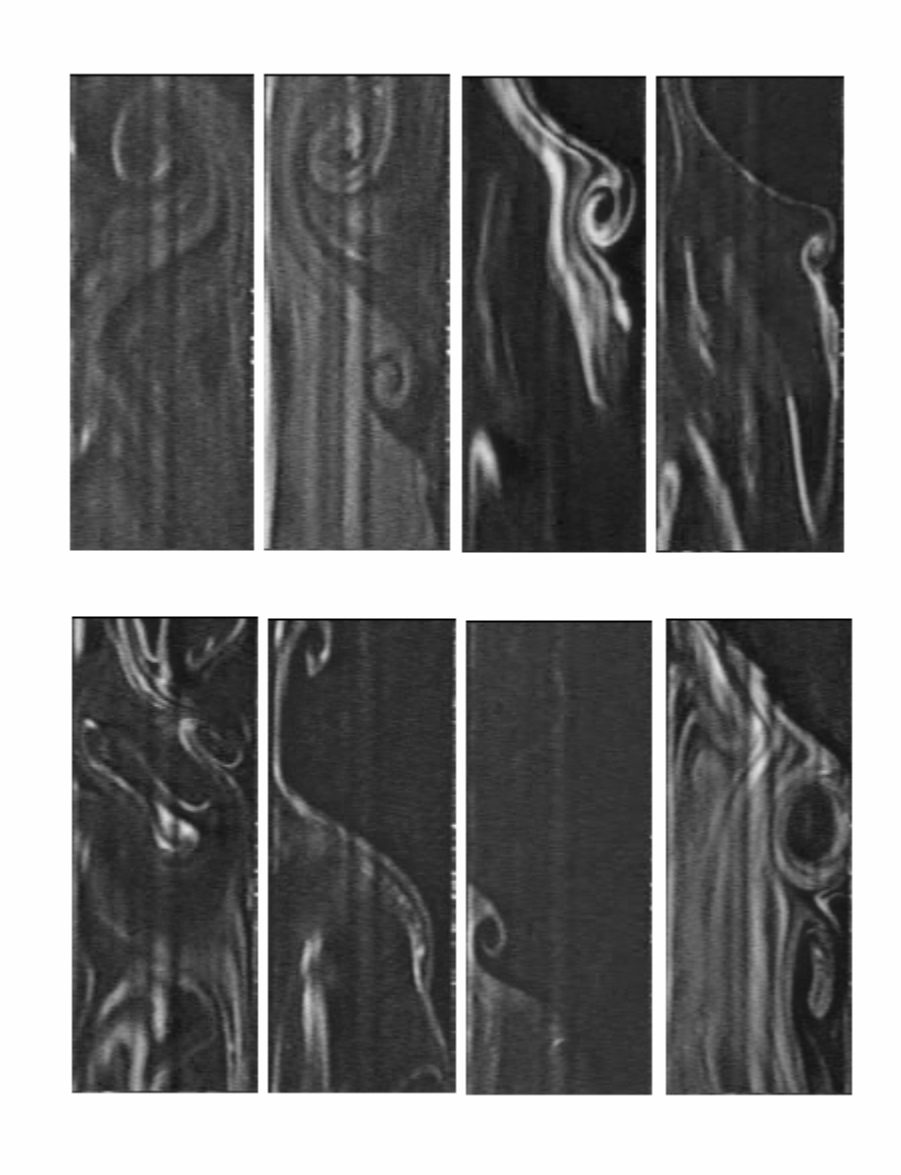

Figure 6: Streak Flow Pattern at Ra=54,800 (fully turbulent)

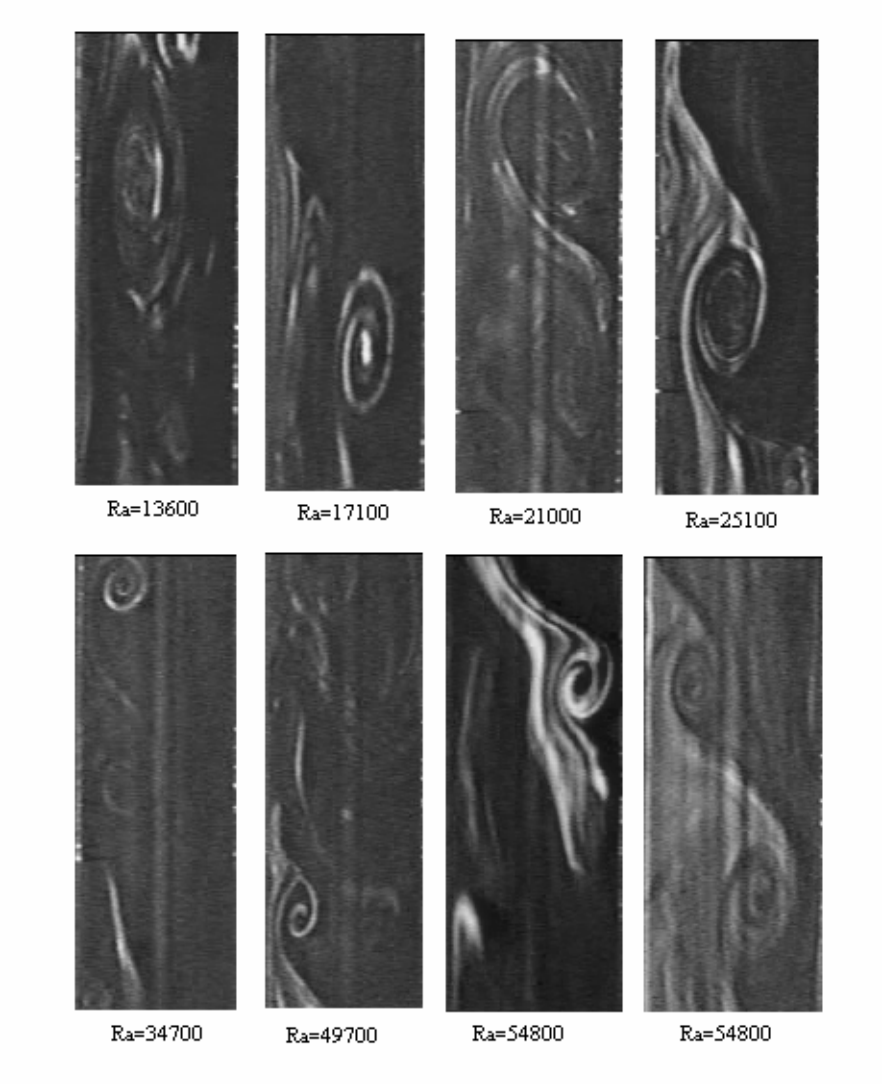

Figure 7: Co-Rotating Cells

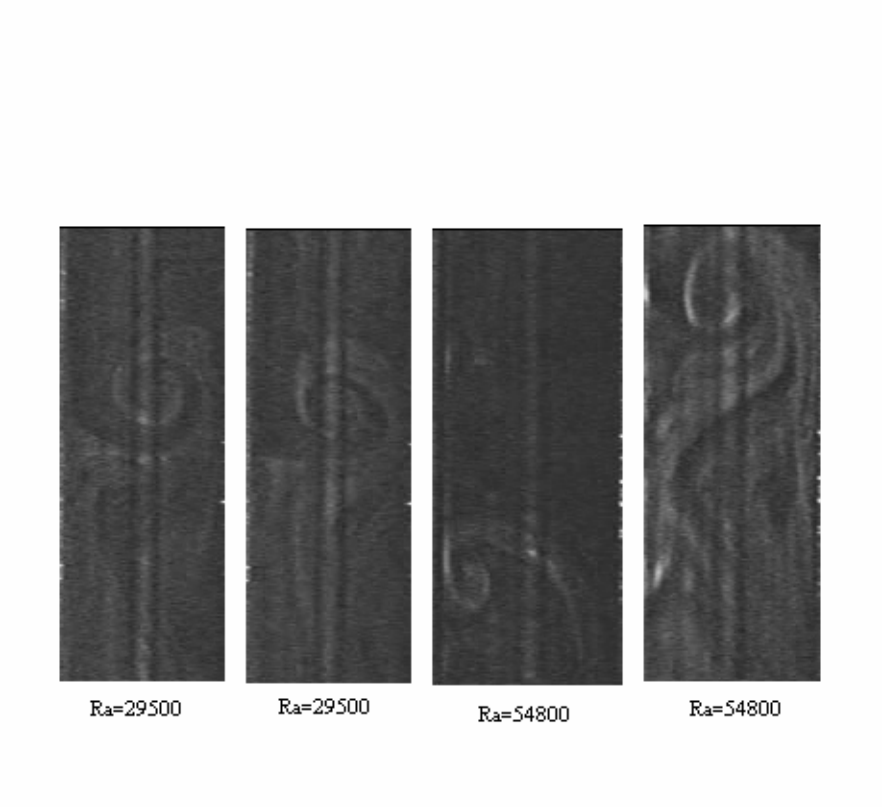

Figure 8: Counter-Rotating Cells

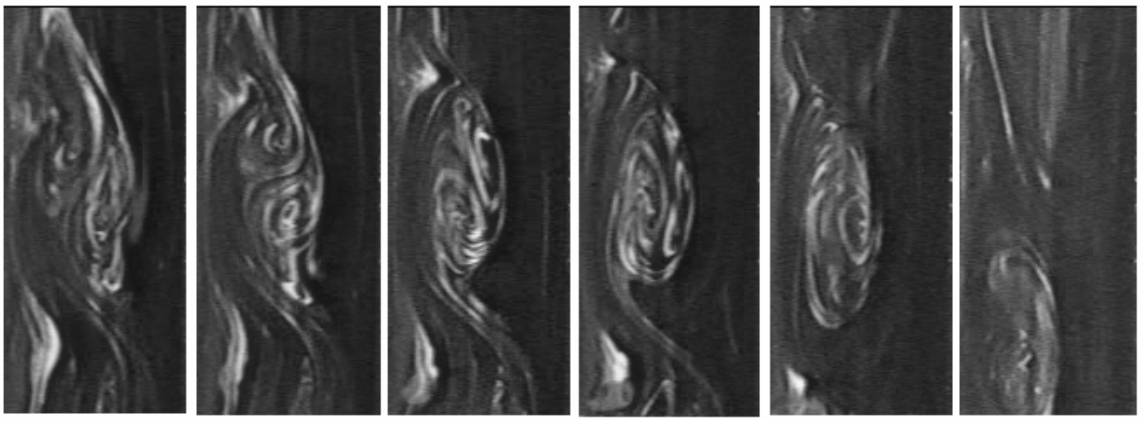

Ra=14700

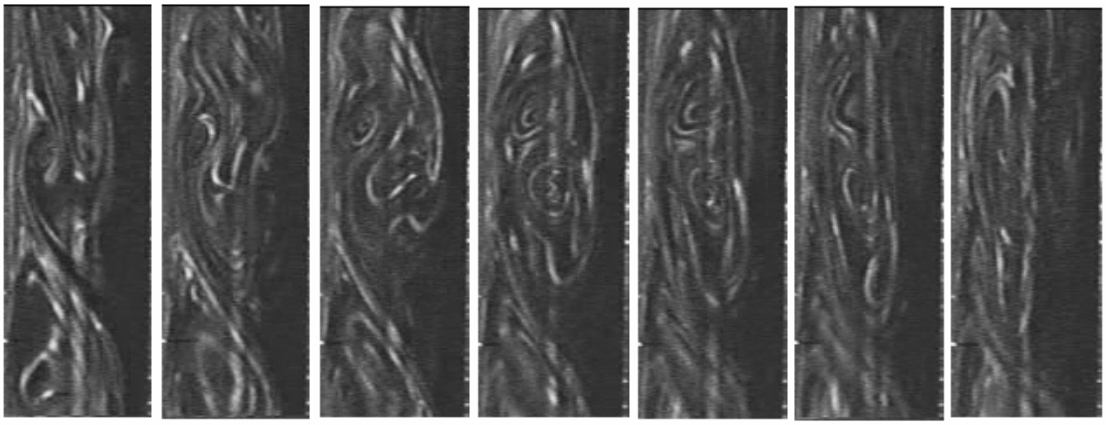

Ra=21000

Figure 9: The Structure of Compound Cells

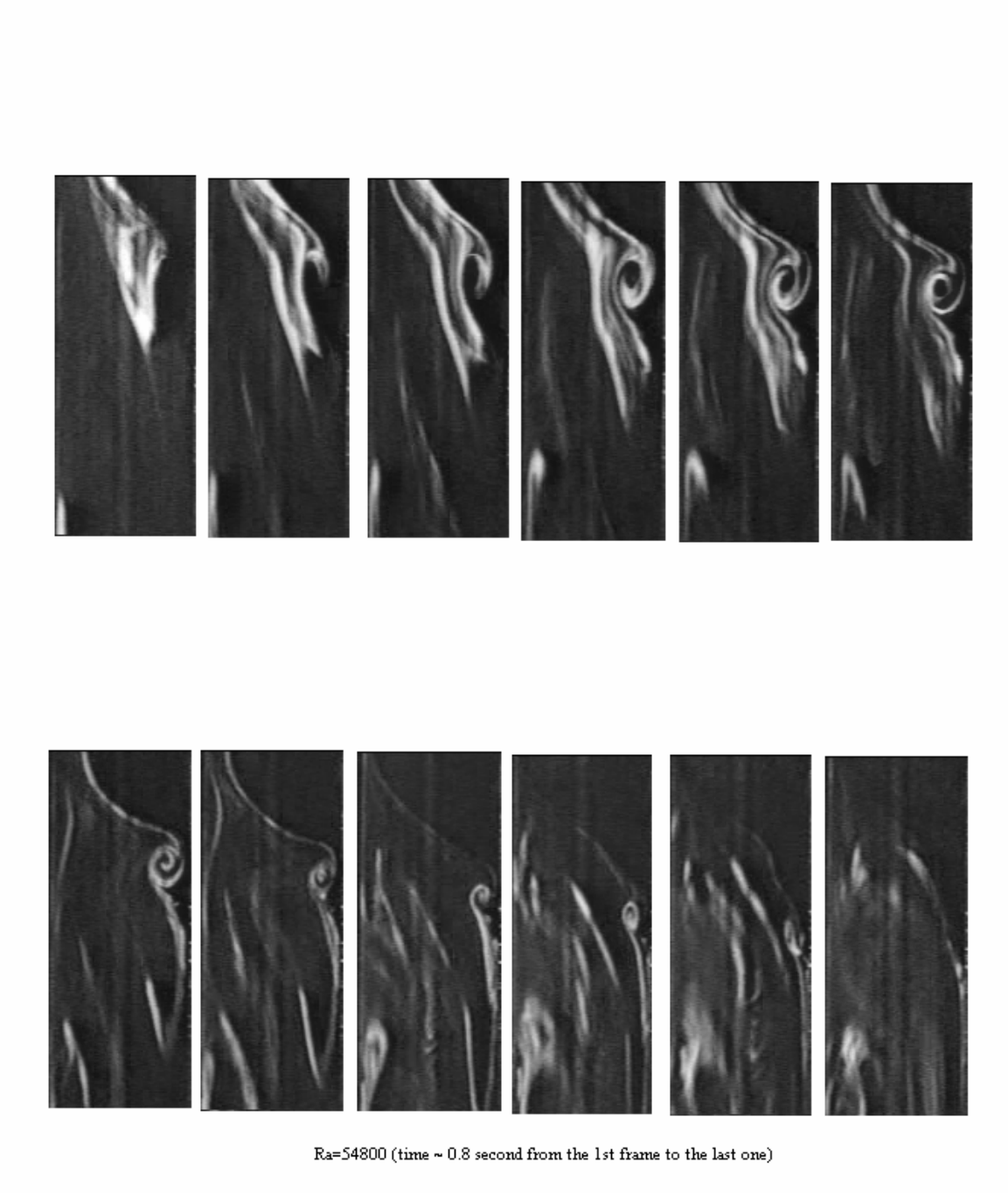

Figure 10: Dissipation of Cells at the Smallest Scales, elapsed time 0.8 seconds

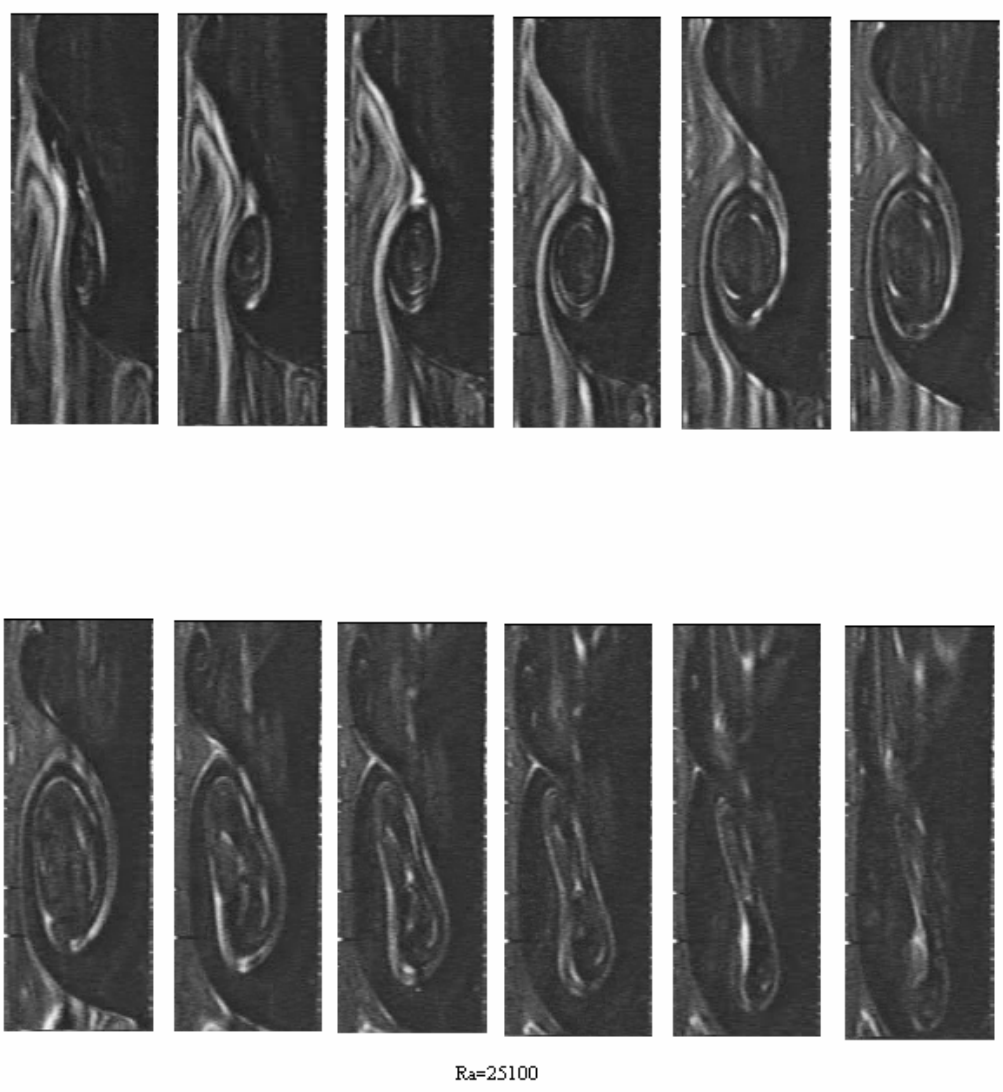

Figure 11: Dissipation of Cells at Larger Scales

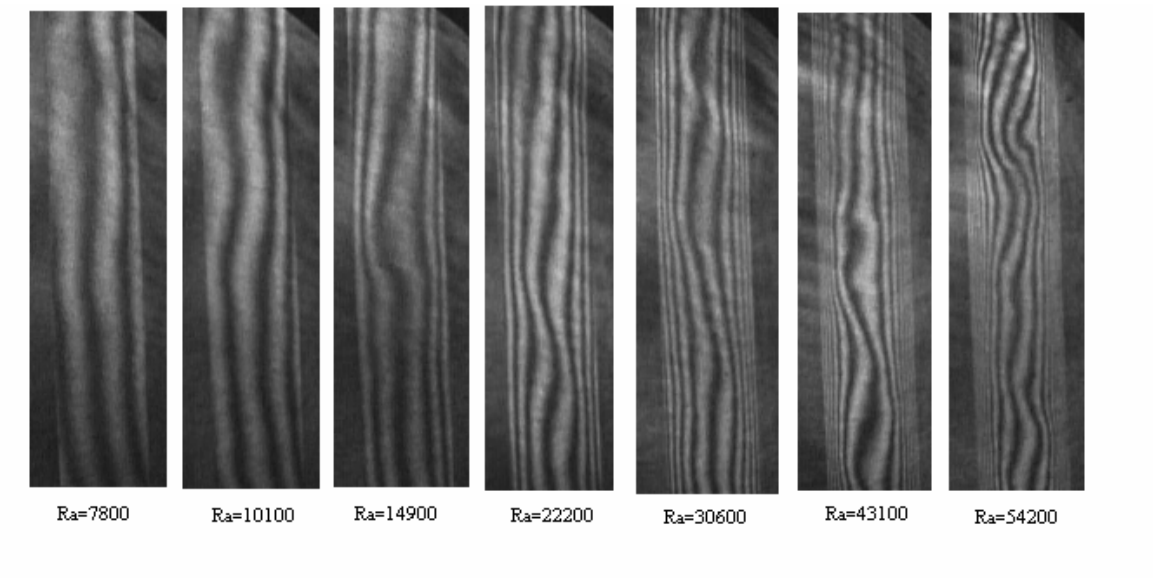

Figure 12: Interferograms of the Middle Section

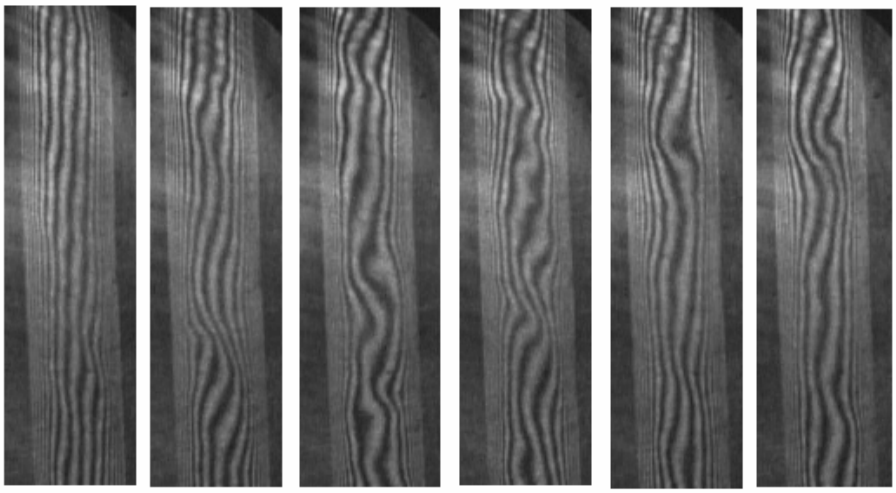

Figure 13: The Variation of Isotherm Patterns at Fully Turbulent Regime (Ra=54,200)

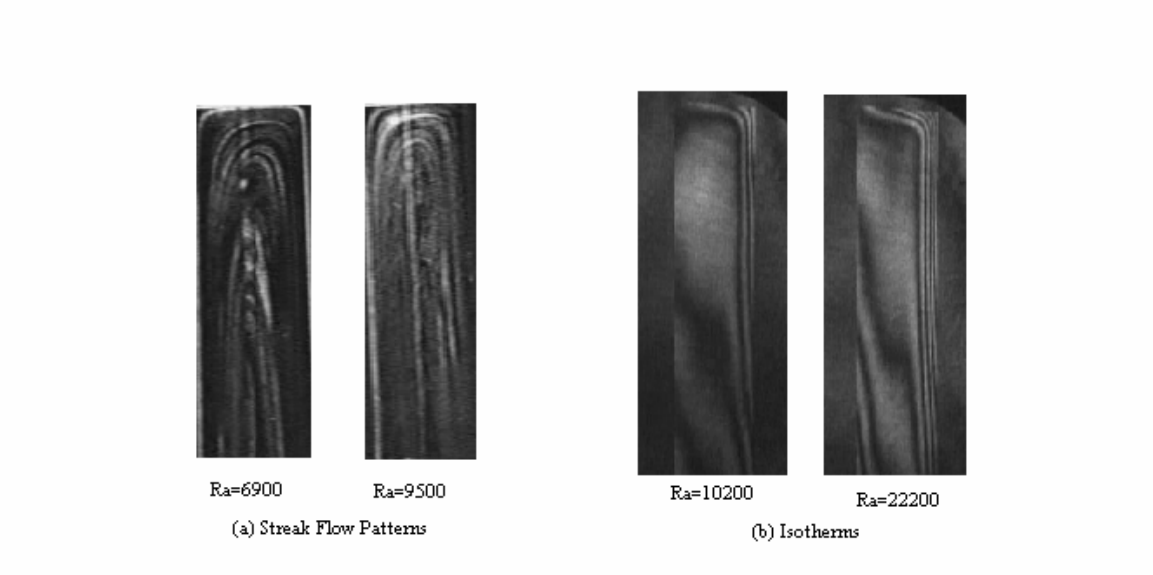

Figure 14: Comparison of Streak Patterns and Isotherms at the Top